Cosmic-Impact Event in Lake Sediments from Central Europe Postdates the Laacher See Eruption and Marks Onset of the Younger Dryas

Gunther Kletetschka,[1,2,3,*] *Daniel Vondrák,*[4] *Jolana Hruba,*[2] *Vaclav Prochazka,*[2] *Ladislav Nabelek,*[1,2] *Helena Svitavská-Svobodová,*[5] *Premysl Bobek,*[5] *Zuzana Horicka,*[6,7] *Jaroslav Kadlec,*[8] *Marian Takac,*[2] *and Evzen Stuchlik*[7]

1. Institute of Geology, Czech Academy of Sciences, CZ-252 43 Průhonice 770, Czech Republic; 2. Institute of Hydrogeology, Engineering Geology and Applied Geophysics, Charles University, Albertov 6, CZ-128 43 Prague 2, Czech Republic; 3. Geophysical Institute, University of Alaska Fairbanks, 903 North Koyukuk Drive, Fairbanks, Alaska 99775-7320, USA; 4. Institute for Environmental Studies, Charles University, Benátská 2, CZ-128 01 Prague 2, Czech Republic; 5. Institute of Botany, Czech Academy of Sciences, Zámek 1, CZ-252 43 Průhonice, Czech Republic; 6. Branch of Applied Ecology, T. G. Masaryk Water Research Institute, Podbabská 30, CZ-160 00 Prague 6, Czech Republic; 7. Institute of Hydrobiology, Biology Centre, Czech Academy of Sciences, Na Sádkách 7, CZ-370 05 České Budějovice, Czech Republic; 8. Institute of Geophysics, Czech Academy of Sciences, Boční II 1401, CZ-141 31 Prague 4, Czech Republic

ABSTRACT

The Younger Dryas (YD) climate episode (~12,850–11,650 calendar years before present [cal BP]) is an event recorded widely across the Northern Hemisphere. We conducted multiple analyses at high resolution of a YD-age sedimentary sequence from Stara Jimka, a paleolake in the Bohemian Forest, Czech Republic. Age-depth modeling indicates that a central European warming trend was interrupted at ~13,020 ± 110 cal BP by the sudden onset of cooling (<20 y) known as the Gerzensee climate oscillation and marked by the deposition of fine-grained sediment at this location. That cooling episode ended at ~13,001 ± 66 cal BP and was followed by a ~121-y-long warming trend. After that, the Laacher See tephra depositional event, dating to ~12,820 ± 20 cal BP, continued an overall warming trend. The composition of Laacher See volcanic tephra in this section likely corresponds to the middle eruption sequence. Finally, the deposition of glassy microspherules marked the onset of the YD climate change at 12,755 ± 92 cal BP. The sequence across the YD onset is marked by (1) a peak in glassy microspherules (>17,000/kg), (2) a peak in framboidal spherules (>4,000/kg), (3) significant changes in the lake's weathering proxies, and (4) major changes in fauna and flora, showing a shift to unfavorable environmental conditions (decrease in temperature and lake trophy status). Collectively, this evidence is consistent with the YD impact hypothesis and evidence of one or more cosmic airburst events occurring at this time.

Online enhancements: appendix.

Introduction

It has been hypothesized that multiple and widespread cosmic impacts/airbursts occurred at the onset of the Younger Dryas (YD) climatic episode, ~12,800 ± 150 calibrated years before 1950 (cal BP), as indicated by extensive evidence at the YD boundary (YDB), which marks the onset of the YD climate change (Firestone et al. 2007; Rasmussen et al. 2014). More than 40 locations spanning 50 million square kilometers across North America, northern South America, Western Europe, and Southwest Asia have been found to contain peaks of microscopic distal-ejecta proxies inferred to be direct evidence of a cosmic-

Manuscript received July 21, 2017; accepted June 18, 2018; electronically published September 24, 2018.

* Author for correspondence; email: kletetschka@gmail.com.

[The Journal of Geology, 2018, volume 126, p. 000–000] © 2018 by The University of Chicago. All rights reserved. 0022-1376/2018/12606-0001$15.00. DOI: 10.1086/699869

This content downloaded from 037.188.230.251 on September 25, 2018 23:51:12 PM
All use subject to University of Chicago Press Terms and Conditions (http://www.journals.uchicago.edu/t-and-c).

impact environment. These proxies include magnetic and glassy spherules, meltglass, fullerenes, nanodiamonds, and platinum-group elements (Firestone et al. 2007; Bunch et al. 2012; Fayek et al. 2012; Israde-Alcántara et al. 2012; LeCompte et al. 2012; Mahaney et al. 2013; Wittke et al. 2013). The less frequent occurrence of scoria-like meltglass is taken as evidence of multiple small-body airbursts/impacts incapable of creating craters that have survived to the present. In addition, evidence of widespread biomass burning associated with an impact event(s) has been reported (Wolbach et al. 2018*a*, 2018*b*), including glass-like carbon, aciform carbon, and carbon spherules. In addition, the well-dated Greenland Ice Sheet Project 2 ice core has a platinum (Pt) anomaly at the onset of the YD cooling episode (Petaev et al. 2013), decades after the generally accepted Laacher See (LS) explosive volcanic eruption in Germany (Baales et al. 2002; Rach et al. 2014). Furthermore, osmium (Os) anomalies with low $^{187}Os/^{188}Os$ ratios were reported for the YDB layer at a North American site and another at Lommell, Belgium, supporting an extraterrestrial episode as the probable cause (Wu et al. 2013). Five independent studies have reported abundance peaks in YDB spherules (references in Bunch et al. 2012; Wittke et al. 2013), while six additional studies at 16 sites have reported YDB nanodiamond accumulations (references in Kennett et al. 2009; Kurbatov et al. 2010; Israde-Alcántara et al. 2012). Even so, the timing of and evidence for the YDB impact hypothesis remain controversial (Pinter et al. 2011; van Hoesel et al. 2014).

Here we report the results of the study of a Late Glacial sedimentary sequence from Stara Jimka (SJ), a former lake in the Bohemian Forest of the Czech Republic (fig. 1). Objectives of this study include determining whether the SJ stratigraphic profile contains (1) evidence of major climate changes, including the Gerzensee climate oscillation (Ammann et al. 2013) and the YD cooling episode at ~12,800 cal BP; (2) tephra associated with a major volcanic eruption in Germany ~12,900 cal BP (LS tephra [LST]); and (3) a layer at the YDB containing high-temperature microspherules (MSPs) and/or other impact proxies, similar to those found at ~40 sites across the Northern Hemisphere that are inferred to have resulted from one or more cosmic-impact events at the YD onset.

Lake Sequence Description and Stratigraphic Settings

The SJ lake catchment today is a steep-faced valley with plateaus on both the western and southern sides. At the end of the Pleistocene, a small glacier probably filled the valley, to be subsequently replaced by rocky glacial erratics. As the ice lobe retreated, it supplied water to the SJ glacial stream, dammed by a landslide two millennia before the YD, at approximately 14,000 cal BP, as inferred from the maximum age of

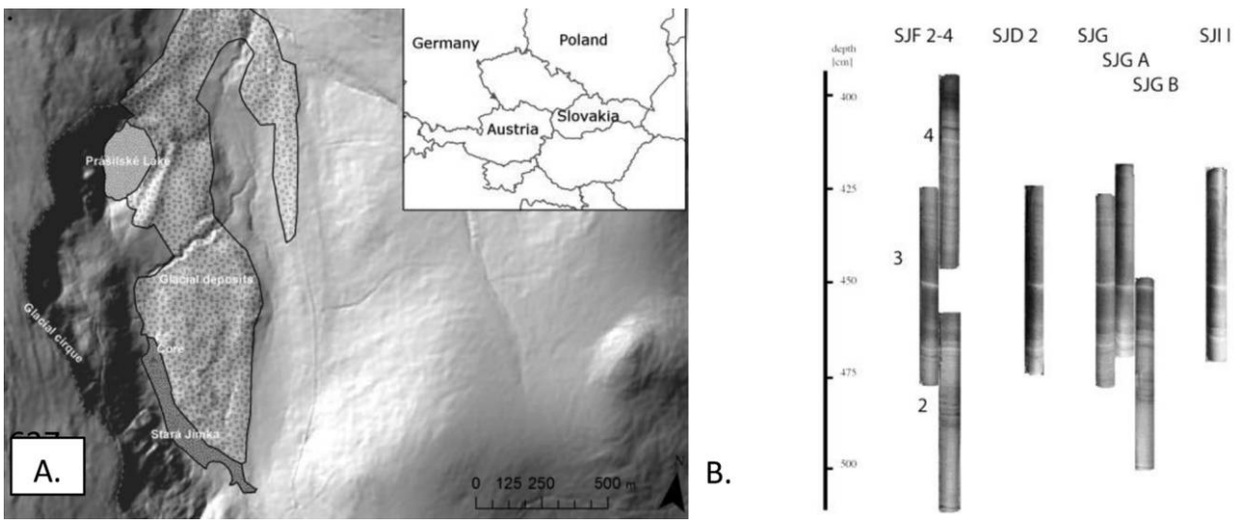

Figure 1. Stara Jimka Lake (lat/long: 49.068722°N/13.402972°E) is situated 20 km southwest of the town of Sušice, Czech Republic. *A*, Site map showing the lake's location (gray triangle in inset) in the paleolake basin. The boundary of the paleolake on a digital terrain model produced from LiDAR (light detection and ranging) data indicates its previous postglacial extent. The extent of glacial deposits is outlined by a solid line enclosing a stippled pattern (modified from Mentlík et al. 2010). *B*, Stratigraphic diagram shows eight overlapping cores taken near the paleolake's maximum depth location. Each core is 50 cm in length, with the deepest penetration being 5 m below ground surface (see "Methods" in the appendix).

This content downloaded from 037.188.230.251 on September 25, 2018 23:51:12 PM
All use subject to University of Chicago Press Terms and Conditions (http://www.journals.uchicago.edu/t-and-c).

the lake sequence (Mentlík et al. 2010). The sedimentary sequence at the SJ lacustrine site is particularly useful in identifying a brief event such as the onset of the YD because the lake has high sedimentation rates, limited bioturbation, and a good ^{14}C chronology and contains a diverse group of microfossils from climate-sensitive lake and catchment organisms (see the appendix, available online).

Results/Discussion

The sequence of SJ glaciolacustrine deposits was collected in eight cores and consists of interbedded silts and clays (figs. 1, A1; figs. A1–A12 are available online; table 1). We used the variations in Rb from X-ray fluorescence (XRF) scans to adjust the depths of individual cores to one unified depth scale ("Methods" in the appendix), with a relative error of ±0.1 cm and absolute error of ±1.0 cm. In addition, a prominent ~1-cm-thick marker layer (451.0–452.4 cm deep) assisted in cross-correlating the depths of the cores. This white layer (designated the "bright varve" [BV]) displayed seasonally stratified sediment that commenced with coarse-grained material (average of ~50 μm) at the bottom of the band and ceased at the top with very fine silt and clay (<5 μm; appendix; fig. A6). The BV, at a depth of 451.0–452.4 cm, is considered a clastic varve, in which coarse layers formed from spring and summer runoff into the lake followed by finer silty layers that formed as fine particles in suspension settled out of the water column during autumn and winter. On the basis of evidence discussed below, we infer that this varve is associated with the sudden Gerzensee cooling oscillation and disturbances in the SJ lake catchment.

To develop an age-depth model, we used Bayesian statistical analysis, which is highly useful (Bronk Ramsey 2009; Kennett et al. 2015) because it allows (1) calculation of millions of possible age models (iterations) that are used to generate an average model, (2) correction of any ages in a sequence that are anomalously old or young, (3) consideration of additional age-specific information (e.g., from archaeology, stratigraphy, palynology, and climatology), and (4) limitation of the uncertainties inherent in ^{14}C dating (Bronk Ramsey 2009). Because of these advantages, we consider Bayesian age-depth modeling more robust and flexible than other types of age-depth models (Parnell et al. 2013). For this study, we used the IntCal13 calibration curve and the OxCal Bayesian analytical program (ver. 4.2.4.; see "Methods").

We acquired four ^{14}C dates from the SJ sequence (bulk sediment, Beta Analytic; table 2; fig. 3; appendix; fig. A3). The oldest date came from a sample about 10 cm below the BV at the depth of 458.6–459.8 cm, and a second ^{14}C sample was taken immediately above the BV (449.8–451.0 cm). A third ^{14}C sample was taken ~2–3 cm above the BV from sediment that is slightly orange in color (448.0–449.0 cm), and the youngest date was for sediment about 35 cm above the BV (413.8–414.8 cm). On the basis of these four ^{14}C dates, we constructed a Bayesian age-versus-depth model (Reimer et al. 2013; table 2; appendix; fig. A3) and obtained calibrated ages of 13,132 ± 44, 12,798 ± 55, 12,683 ± 27, and 11,435 ± 160 cal BP (table 2). The age of 12,798 ± 55 cal BP just above the BV postdates the reported date (~12,900 BP) of the LS eruption and LST deposition in Europe (Brauer et al. 1999). The calibrated age of the orange layer containing LST material, 12,683 ± 27 cal BP (448.0–449.0 cm), has to be adjusted about 200 y older because this is, in fact, the marker horizon for the LS eruption (Wulf et al. 2013) documented as 12,880 ± 20 cal BP in table 2 (Bogaard and Schmincke 1985).

A radiocarbon date with a modeled age of 11,435 ± 160 cal BP (table 2) was acquired from the shallowest depth of 414.4–415.0 cm and was used to obtain an accumulation rate of ~36.4 ± 5 y/cm between 414.4 and 448.6 cm. Similarly, we calculated a deposition rate of 60.5 ± 8.6 y/cm for the centimeter of sediment between the orange LST material layer and the BV (table 2). The BV displayed a very rapid deposition rate of 1 cm for every 1–2 y. Sediment below the BV

Table 1. Sedimentary Cores (50 cm) Collected by the Russian Chamber Corer for Specific Proxy Analysis

Core	Depth (cm)	^{14}C dates	XRF	LOI	MS	Microspherules	LS glassy shards	Pollen, algae	Charcoal	Chironomids	Cladocerans
SJF 2	445.0–498.2				x	x					
SJF 3	373.2–422.0		x		x	x	x			x	x
SJF 4	396.8–443.6	1	x								
SJD 2	425.4–471.4	2	x	x				x	x		
SJG	448.0–498.2		x								
SJG A	419.3–469.9		x	x							
SJG B	443.7–453.9		x				x				
SJI I	443.6–455.8	1	x				x				

Note. XRF = X-ray fluorescence analysis; LOI = loss on ignition; MS = magnetic susceptibility; LS = Laacher See.

This content downloaded from 037.188.230.251 on September 25, 2018 23:51:12 PM
All use subject to University of Chicago Press Terms and Conditions (http://www.journals.uchicago.edu/t-and-c).

Table 2. Accelerated Mass Spectrometry Radiocarbon and Modeled Ages for the Stara Jimka Paleolake Profile, with Notes Related to the Weathering Profile in Figure 3

	^{14}C age ± 1σ (cal BP)	Depth ± 1σ (cm)	Modeled age						Accumulation rate ± 1σ (y/cm)
			μ (BP)	68.20%	95.40%	Agreement index	Convergence integral	LST corrected (BP)	
Top of core	9980 ± 50	414.3 ± 1.00	11,435	160	221	97.9	95.7	11,602	36.4 ± 5.0
End of third stage of YD		442.6 ± 1.00	12,470	143	307			12,637	36.4 ± 5.0
Third stage of YD		443.0 ± 1.00	12,480	136	300			12,647	36.4 ± 5.0
End of second stage of YD		445.2 ± 1.00	12,560	92	232			12,727	36.4 ± 5.0
Second stage of YD + MSPs		446.0 ± 1.00	12,590	82	218			12,757	36.4 ± 5.0
End of first stage of YD		447.6 ± 1.00	12,650	41	129			12,817	36.4 ± 5.0
First stage of YD		448.4 ± 1.00	12,680	27	68			12,847	36.4 ± 5.0
Center of LST layer	10,720 ± 40	448.5 ± 1.00	12,683	27	61	107.6	98.9	12,850	60.5 ± 8.6
Onset of LST		449.0 ± 1.00	12,713	44	109			12,880	60.5 ± 8.6
Just above BV	10,970 ± 50	450.4 ± 1.00	12,798	55	116	117	98.8	12,965	60.5 ± 8.6
End of BV		451.0 ± 1.00	12,834	66	142			13,001	.7 ± .1
Start of BV		452.4 ± 1.00	12,835	66	142			13,002	.7 ± .1
Bottom of core	11,270 ± 50	459.2 ± 1.00	13,132	44	95	94.6	96.3	13,299	38.0 ± 6.2

Note. ^{14}C dates (dating by Beta Analytic, Miami) were calibrated with OxCal, version 4.2.4. The depth 414.3 cm corresponds to a 1-cm-thick layer subjacent to the onset of Holocene organic sedimentation. The depth 448.5 cm is the center of the layer containing Laacher See tephra (LST). The depth 450.4 cm is immediately above the white lamina (BV) in the core, interpreted as a cooling event due to Gerzensee oscillation. The depth 459.2 cm is near the beginning of the grayish-brown gyttja ("Core Sediment Composition" in the appendix). Four radiocarbon ages constrain three accumulation rates of the sediment between them (last column). For the individual agreement index and the convergence integral of the Bayesian model, high values (>60) indicate that the model is a good statistical match. The "LST corrected" column shows all age values recalculated according to the onset of LST-corrected marker horizon and the known age (12,880 cal BP) of the LS eruption (Bogaard and Schmincke 1985). YD = Younger Dryas, MSPs = microspherules, BV = bright varve in the middle of the presumed Gerzensee oscillation.

This content downloaded from 037.188.230.251 on September 25, 2018 23:51:12 PM
All use subject to University of Chicago Press Terms and Conditions (http://www.journals.uchicago.edu/t-and-c).

had a slower accumulation rate of 1 cm for every 38.0 ± 6.2 y (table 2).

The ages of the sampled sequence of SJ sediment overlap ages for the deposition of LST from the East Eifel Volcanic Field across parts of northern Europe, mainly in Germany, France, and Switzerland; no sites have been previously reported in the Czech Republic. The LS explosive volcanic event (Rausch et al. 2015) is estimated to have continued for at least 10 d and may have triggered a sudden cooling event that may have lasted for few years in central Europe. This cooling event would be caused by the atmospheric injection of large amounts of aerosols that blocked solar radiation (Baales et al. 2002). In addition, the solar absorption by the lofted volcanic aerosols heated the upper levels of the atmosphere, creating a high-pressure cell that diverted the jet stream, bringing cold air farther south in Europe (Robock 2000).

Electron Microscopy and Geochemical Analyses

Using scanning electron microscopy (SEM), we conducted analyses of thin sections of core sediment (core SJI I) and discovered small glassy fragments of apparent volcanic tephra displaying characteristic gas vesicles. Analyses by energy-dispersive X-ray spectroscopy (SEM-EDS; see "Methods") reveal that one layer contains significant amounts of glassy shards with compositions matching tephra from the LS eruption (fig. 2; appendix). The group of fine-grained material at SJ forms the BV layer and dates to ~12,834 ± 66 cal BP (451.0 cm; table 2), an age that is close to the Gerzensee climate oscillation at ~13,000 cal BP (Ammann et al. 2013; van Raden et al. 2013). This BV layer is visible in all cores. It is easily identified by XRF analyses that show peaks in concentrations of Fe, Al, and K, reflecting a sharp decline in the amount of organic material (fig. 3; appendix), which indicates a reduction in biotic productivity in the lake and/or increased transport of inorganic matter from the catchment at that time. Altogether, it appears that a significant cooling event occurred. A similar cooling-episode signal was probably found in the southern part of the Czech Republic at Švarcenberk Lake, where an independent study shows a similar increase in Rb concentrations, changes in magnetic susceptibility, and a decrease in organic content, as indicated by loss-on-ignition (LOI) values (Hošek et al. 2014).

Above the BV layer, after deposition of 3 cm of sediment representing a duration of ~121 y (table 2), there is tephra layer that dates to ~12,713 ± 44 cal BP (449 cm). Although the Bayesian age-depth model indicates that this tephra layer may have been deposited at the YD onset, making this layer analogous to the YDB layer that is recognized elsewhere dating to ~12,800 ± 150 cal BP (Firestone et al. 2007;

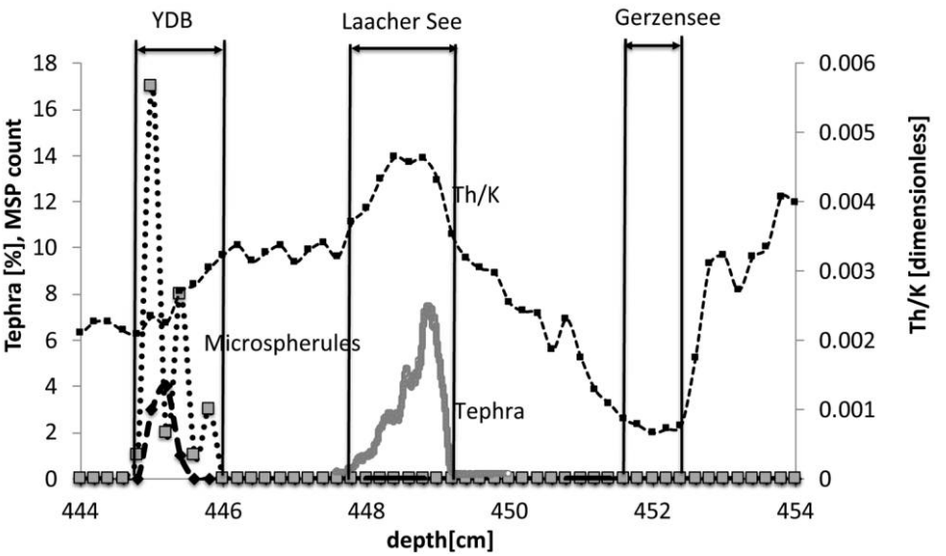

Figure 2. Occurrence of tephra particles and glass in core SJI and framboidal iron-enriched microspherules (MSPs) in core SJF 3. Concentration of tephra grains (gray curve) was determined with scanning electron microscopy across a 1 × 50-mm thin section from core SJI I (see "Methods" in the appendix). The dashed curve shows weathering parameter Th/K (Taylor et al. 2006). Three pairs of solid black lines with arrows defining their width along the depth axis correspond to the three older ^{14}C dates: the Gerzensee oscillation, the Laacher See tephra, and the Younger Dryas boundary (YDB), with the latter marking the appearance of proxies of the YDB impact event at onset of Younger Dryas. Abundances of MSPs and framboids from cores SJF 3 are depicted by squares along the dotted curve and by diamonds along the dashed curve.

This content downloaded from 037.188.230.251 on September 25, 2018 23:51:12 PM
All use subject to University of Chicago Press Terms and Conditions (http://www.journals.uchicago.edu/t-and-c).

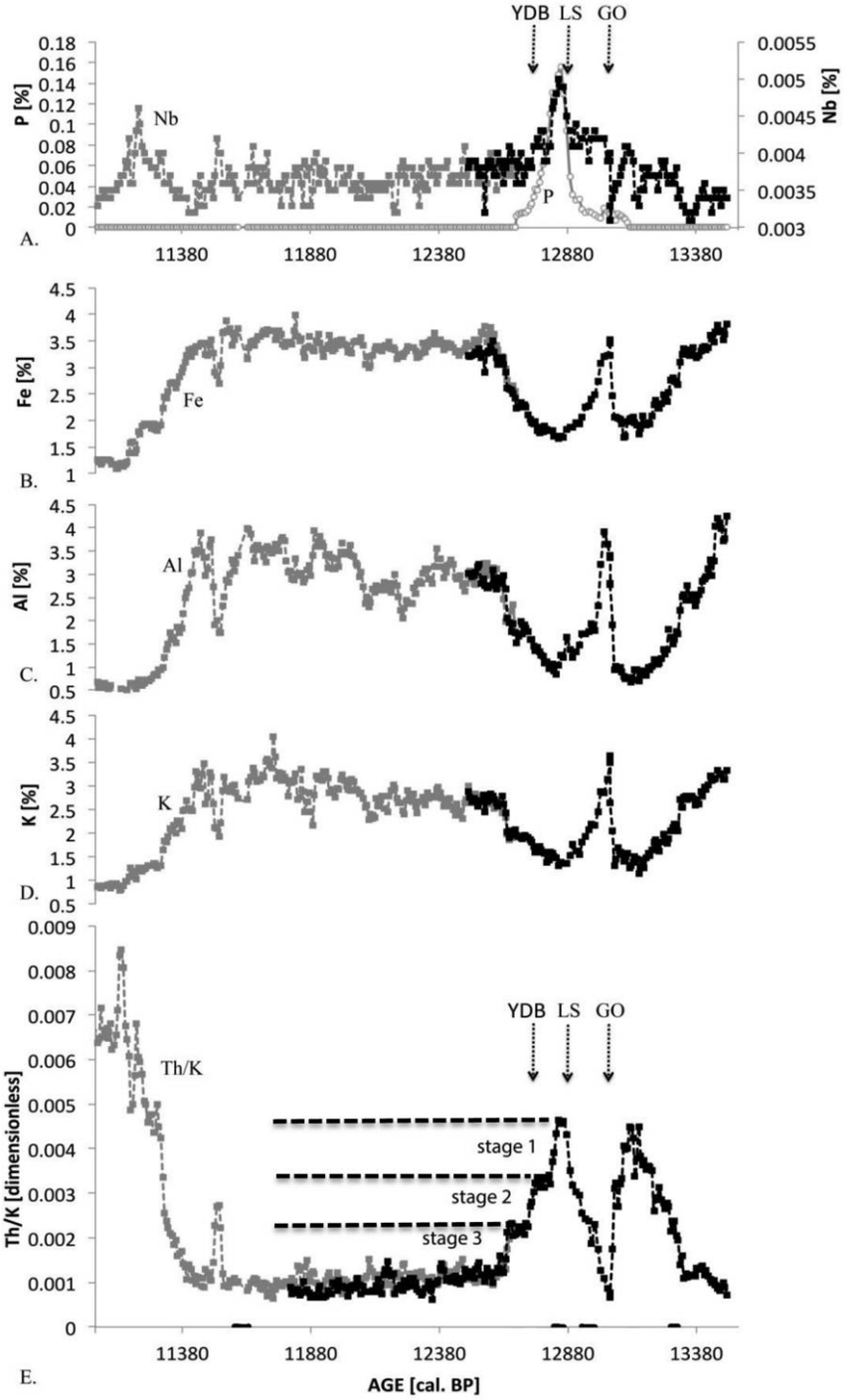

Figure 3. Chronological variation of relative concentrations in P, Nb, Fe, Al, and K and Th/K across the sedimentary section that contains the Younger Dryas (YD) onset (core SJG A). Short black bars along the age axis show where the ^{14}C dates were obtained. "GO" identifies the Gerzensee oscillation, "LS" indicates the onset of the Laacher See tephra deposition in the core, and "YDB" indicates the presence of microspherules marking the YD boundary impact event and the YD onset. Horizontal lines in *E* show three stages of geochemical changes during the Allerød-YD transition (see text).

This content downloaded from 037.188.230.251 on September 25, 2018 23:51:12 PM
All use subject to University of Chicago Press Terms and Conditions (http://www.journals.uchicago.edu/t-and-c).

Kennett et al. 2009; Bunch et al. 2012; LeCompte et al. 2012; van Hoesel et al. 2012; Mahaney et al. 2013), its composition clearly indicates that the tephra is from an LS eruption the original of which is dated by varve and tree ring chronologies to 12,880 ± 20 cal BP (Bogaard and Schmincke 1985). If so, this means that the inferred age-depth model is likely to be too young by up to 200 y. Detailed analysis of material in this upper tephra layer revealed melted glassy shards containing gas vesicles (fig. 4) and euhedral clinopyroxene crystals (appendix). The geochemical composition of this tephra matches the LS volcanic tephra from the middle sequence of the LS eruption (table 3; appendix; Schmincke et al. 1999). The occurrence of this material constrains the age of this sediment.

Above the initial orange-colored tephra layer, we found high-temperature MSPs in a concentration of >17,000/kg, a quantity of MSPs much higher than those reported from >40 YDB sites (average of ~400 spherules/kg). Some of the iron-enriched high-temperature MSPs contain small amounts of nickel (fig. A9), consistent with incorporation of material from the impactor or from Ni-enriched target rocks. The abundance peak in high-temperature-related MSPs in a distinct layer near the YD onset (fig. 2) also coincides with a peak in diagenetic framboids. The two types of MSPs (glassy and iron enriched) are similar to those of the same age widely reported in the YDB layer across several continents (Bunch et al. 2012; Wittke et al. 2013). The geochemical composition of these MSPs and their dendritic structure (appendix) are inconsistent with volcanic, cosmic, authigenic, diagenetic, or anthropogenic origins but rather are morphologically and chemically similar to MSPs produced by known impact events (Bunch et al. 2012; Wittke et al. 2013).

The YDB MSPs have been the subject of considerable controversy about their origin, and although some researchers have claimed that YDB MSPs are not impact related, no one has as yet offered a viable alternative explanation for their presence (Pinter et al. 2011). The SJ MSPs are ~3 cm above the LST, and it is highly unlikely that they resulted from the LS eruption, because a previous examination of three samples of LST found no MSPs of any kind (Moore et al. 2017) and because MSPs are not known to be directly formed by explosive volcanism (Moore et al. 2017). In addition, no MSPs were found associated with the lower tephra layer, strongly suggesting that the formation of MSPs at SJ is unrelated to volcanism.

On the other hand, MSPs can be produced by lightning strikes (Shevtsov et al. 2016), which are the only natural process other than cosmic impact that generates sufficiently high temperatures to melt iron into spherules (French 1998). To test the possibility that some SJ MSPs formed by lightning, we separated a few MSPs by nonmagnetic methods and tested them for remanent magnetism, which is induced in iron-rich objects by lightning strikes. All YDB MSPs display dendritic texturing, indicative of high-temperature melting (>1450°C), and were separated from sediment containing abundant tephra particles. We identified two MSPs with sufficient amounts of magnetism to allow testing for the presence or absence of lightning remanent magnetization (LRM; Wasilewski and Kletetschka 1999). One MSP did not display significant LRM, indicating that it did not result from a lightning strike. The other MSP contained significant LRM, providing indirect evidence of formation by lightning (Wasilewski 1981; Wasilewski and Kletetschka 1999), thus suggesting that at least a portion of the MSPs in SJ could have been created by lightning strikes.

Here is one hypothetical explanation of these results. Airbursts/impacts lofted into the air impact-related melted MSPs, dust, and vaporized ground cover. Then, lightning strikes within the impact cloud melted some of these particles to create MSPs displaying LRM (Shevtsov et al. 2016). The presence of MSPs in the YDB layer at the SJ site (fig. 4*B*–4*D*) provides indirect support for this hypothesis, which explains all the various characteristics of the MSPs found at SJ.

Compositional XRF analysis across the BV layer identified elevated concentrations of major rock-forming elements (Fe, K, Al; fig. 3). We infer that changes in temperature and precipitation during the Gerzensee oscillation (GO; Ammann et al. 2013; van Raden et al. 2013) resulted in an erosional event in the lake catchment and a sharp increase in the sedimentation rate. This change is evident as a gradation from coarser-grained sediment deposited during summer to finer-grained sediment deposited during winter.

Plotting the weathering index Th/K (Taylor et al. 2006), along with major elements (K, Al, Fe, and P), by age (fig. 3) shows that concentrations of tephra particles (fig. 2) correlate with a significant peak in Th/K values (fig. 3). We infer that the LST deposition did not change the overall warming trend after the Gerzensee cold oscillation at the SJ site. The decrease in Th/K toward the YD onset postdates the LST accumulation. The increase in Th/K values in the lower part of the core, just before 13,299 ± 44 cal BP, marks the beginning of soil production in the SJ catchment. The first onset of LS accumulation, at 13,002 ± 66 cal BP, parallels a sharp decline in Th/K values, indicating a sudden change toward dry and/or cold conditions (Pliler and Adams 1962) consistent with the Gerzensee cold oscillation (Ammann et al. 2013; van Raden et al. 2013). In this specific case, the change

This content downloaded from 037.188.230.251 on September 25, 2018 23:51:12 PM
All use subject to University of Chicago Press Terms and Conditions (http://www.journals.uchicago.edu/t-and-c).

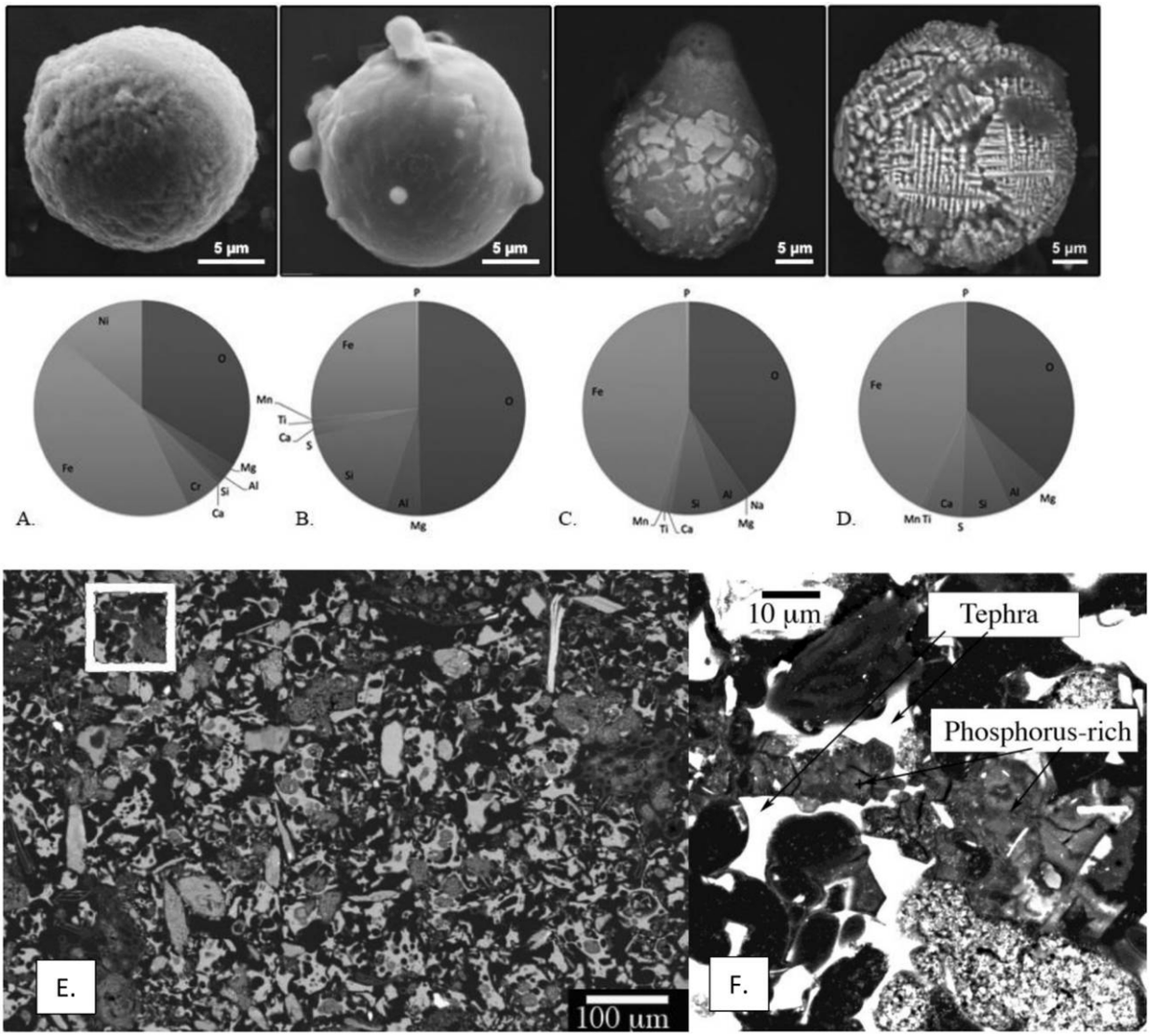

Figure 4. Microspherule (MSP) morphologies (scanning electron micrographs), chemical compositions, and thin-section images. *A*, Iron-enriched MSP containing nickel. *B*, Glassy MSP with melted droplets accreted to its surface. *C*, Glassy droplet with crustal plates of rapidly quenched iron. *D*, Iron-rich MSP with skeletal, quenched texture. *E*, Polished thin section showing vesicular tephra shards dating to the Younger Dryas onset. The rectangle outlines image *F*. *F*, Phosphorus-rich aerosol grain incorporated within tephra glass. Images were taken with a scanning electron microscope using back-scattered electrons.

is associated with increased accumulation of inorganic particles due to instability within the surrounding soil, which resulted from rapid cooling during the Gerzensee event at 13,002 ± 66 cal BP (fig. 2). The Th/K values then climbed quickly because soils in SJ area were already developed before LS cooling.

After the onset of the LST accumulation, the trend of increasing Th/K values ceased abruptly, and Th/K started declining as the climate became dryer and colder (fig. 3). However, the decline is not in one but in three stages. During the second stage, at 12,757 ± 82 cal BP, we have a second dip in Th/K, along with the appearance of MSPs, both glassy and framboidal, marking the onset of the YDB layer, as identified elsewhere (Bunch et al. 2012; Wittke et al. 2013). The low Th/K values persisted for ~1380 y, after which Th/K rebounded to high values at a depth of ~409 cm (~1300 cal BP; using the accumulation rate of 36 y/cm in fig. 3). This is also the period when Holocene forest soil formed in the SJ catchment. The YD ended at

This content downloaded from 037.188.230.251 on September 25, 2018 23:51:12 PM
All use subject to University of Chicago Press Terms and Conditions (http://www.journals.uchicago.edu/t-and-c).

Table 3. Mean Electron Probe Microanalysis (EPMA) Tephra Glass Data from Younger Dryas Boundary Sediment Section of Stara Jimka in Comparison with Distal LST Units from Various Sites across Central and Northern Europe

	MLST-C	MLST-B, MLST-C	MLST-B, MLST-C	ULST	MLST-B, LLST	MLST-B, LLST	MLST-C	MLST-C	MSPSJ
Site	Tr #1	Re #2	Re #1	Me #2	Wa #3	Ni #3	Da #4	Va #5	
Location	Trzechovskie Lake	Rehwiese Lake	Rehwiese Lake	Meerfelder maar	Warnowo Lake	Niechorze	Daschower	Vallensgård	Stara Jimka
Reference	Wulf et al. 2013	Neugebauer et al. 2012	Wulf et al. 2013	Neugebauer et al. 2012	Juvigné et al. 1995	Juvigné et al. 1995	Riede et al. 2011	Turney et al. 2006	This study
n	1	18	24	22	9	14	1	15	40
SiO_2	62.03	59.01	60.15	60.63	57.19	58.52	60.14	60.35	58.82
TiO_2	.43	.29	.27	.60	.16	.20	.52	.47	.20
Al_2O_3	19.20	21.79	22.10	20.61	23.13	21.70	20.05	20.78	23.10
FeO total	2.88	1.92	1.79	2.29	1.84	1.85	2.24	2.15	1.82
MnO	.22	.27	.22	.16	.45	.45	.16	.08	.29
MgO	.38	.11	.13	.42	.07	.07	.29	.23	.08
CaO	1.80	1.05	1.32	1.94	.49	.65	1.61	1.64	.87
Na_2O	5.48	9.48	7.90	5.72	12.10	10.90	7.33	7.45	8.73
K_2O	6.87	6.09	5.81	7.52	4.52	5.65	7.27	6.85	5.69
P_2O_5	.03	.03	.01	.10	NA	NA	.10	NA	.03
Cl	.79	.37	.33	NA	NA	NA	.32	NA	.41
F	.12	.00	.09	NA	NA	NA	.08	NA	.24
Total[a]	100.23	100.41	100.12	99.99	99.95	99.99	100.11	100.00	100.28
Correlation	.995	1.000	1.000	.996	.998	.999	.998	.998	1

Note. The composition details about the standards used for the analysis of the Laacher See tephra (LST) in the Stara Jimka paleolake (MSPSJ) are provided in the appendix. The "correlation" row indicates the degree of correlation between the EPMA data for the tephra containing MSPs (MSPSJ) and data from the other sites. Note that as a result of the use of a small beam size (5 μm), slightly elevated SiO_2 and lower Na_2O concentrations occur for these samples, suggesting sodium migration during EPMA. LLST, MLST, and ULST denote the lower, middle, and upper LST, respectively. NA = not available.

[a] Normalized to oxide 100%.

This content downloaded from 037.188.230.251 on September 25, 2018 23:51:12 PM
All use subject to University of Chicago Press Terms and Conditions (http://www.journals.uchicago.edu/t-and-c).

~11,650 cal BP (Rasmussen et al. 2014), and it took local soils ~350 y to reach maturation.

Geochemical analyses of LST sediments revealed significant anomalies in phosphorus, calcium, and niobium (fig. 3), whose peak concentrations correlate with high concentrations of tephra shards. Niobium content is stable in sediment across the core intervals and does not vary with climate, but it displays higher values within the tephra accumulation layers. The input of nonlocal material into the lake is indicated by higher concentrations of lanthanum and cerium, rare earth elements, which correlate with the tephra deposits (appendix).

Evidence exists for widespread biomass burning at the onset of the YD that is contemporaneous with the YDB layer across North America and western Europe (Firestone et al. 2007). At the SJ site, we observed only a small increase in charcoal beginning within the YDB layer, indicating a modest increase in biomass burning at the YD onset in the lake's vicinity (fig. A5*A*). However, there is evidence of a very large increase in phosphorus within the tephra-rich LST layer (figs. 3, 5). The LST shards contain less than 0.01% phosphorus (table 2) and therefore cannot account for the increase in phosphorus in lake sediment. Detailed geochemical analyses show that

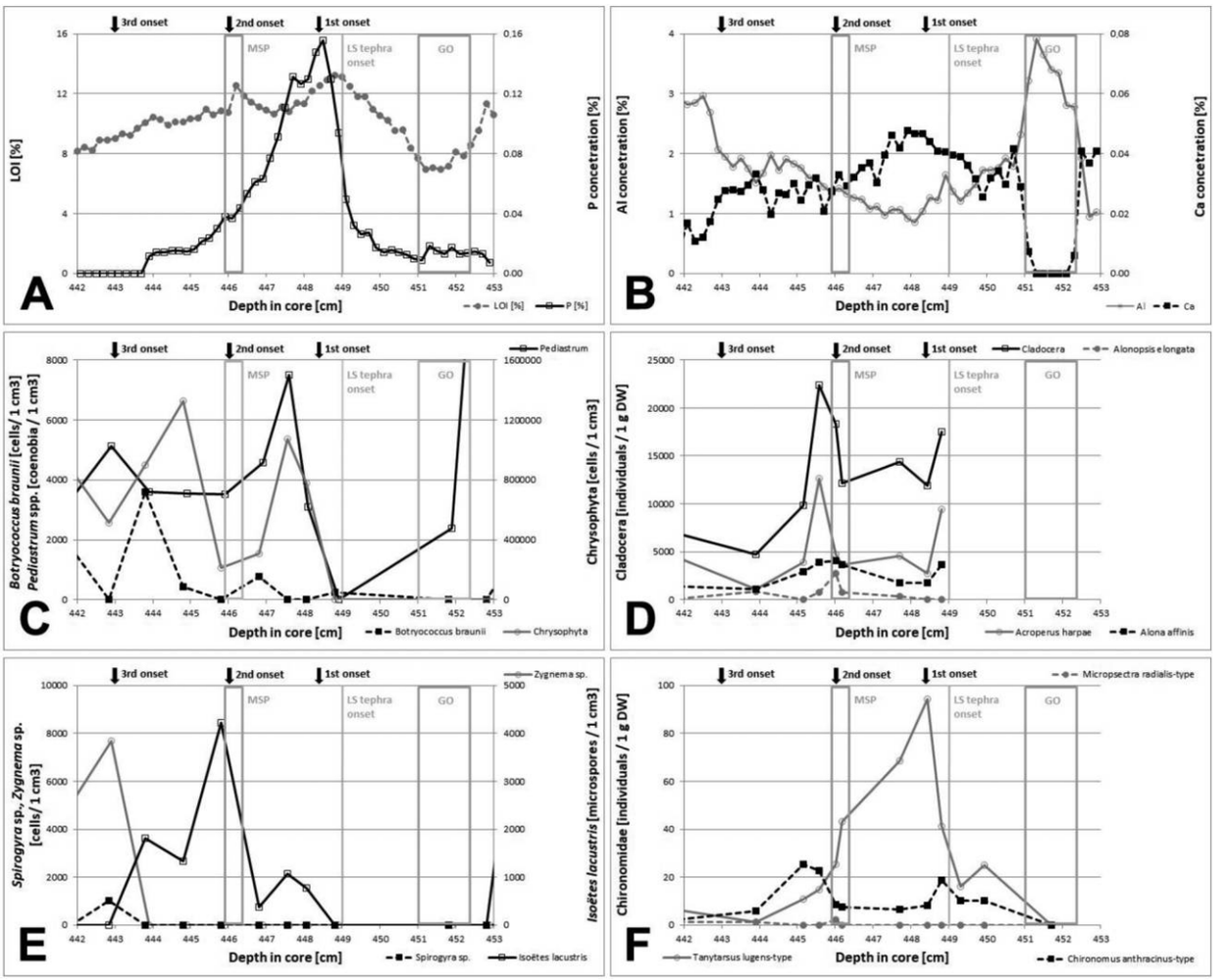

Figure 5. Sediment record from Stara Jimka showing the biological responses to the Gerzensee oscillation (GO), the onset of Laacher See (LS) tephra deposition, and the Younger Dryas boundary indicated by glassy microspherules (MSP). The onsets of the three Younger Dryas stages identified in figure 3 are distinguished by vertical arrows above the diagrams. The GO corresponds to the bright erosion layers with clastic varve-like morphology. *A*, Variation in phosphorus (by X-ray fluorescence [XRF]) and loss on ignition (LOI). *B*, Variations in aluminum and calcium determined by XRF. *C*, Response of selected lake planktonic algae. *D*, Response of selected cladocerans. *E*, Response of benthic algae and quillwort *Isoëtes lacustris*. *F*, Response of selected chironomid taxa. DW = dry weight.

This content downloaded from 037.188.230.251 on September 25, 2018 23:51:12 PM
All use subject to University of Chicago Press Terms and Conditions (http://www.journals.uchicago.edu/t-and-c).

sediment lacking tephra contains about 300 mg/kg of phosphorus (table A2; tables A1, A2 are available online), whereas the sediment containing peak concentrations of tephra exhibits phosphorus concentrations of >2400 mg/kg. Thus, the phosphorus enrichment of 2100 mg/kg is associated with the LST deposition but is not contained within the tephra shards. In investigating this, we found discrete phosphorus-rich grains (PRGs) mixed within the tephra-rich sediment of the LST layer (fig. 4*F*). These PRGs appear to be composed of life-forming (i.e., biotically derived) elements (N, O, C, P) mixed with major elements commonly found in upper soils (Si, Al, S, Fe; figs. 4*F*, A11*B*). Large PRGs were found to have bonded to LST particles, suggesting that they were large aerosols that adhered to LST particles as they became airborne (fig. 4*F*). The existence of these PRGs as aerosols supports the hypothesis that the LS eruption occurred in a preexisting lake and/or a densely vegetated area.

We offer this hypothetical scenario for the origin of the YDB layer. One or more hypothesized airburst events, similar to the Tunguska event (Badyukov et al. 2011; Kletetschka et al. 2017), would have incinerated exposed organic cover (grass, leaves, and wood) and lofted the resulting debris into the atmosphere. Large amounts of atmospheric dust and water vapor, produced and lofted during an airburst event, could have produced lightning discharges (Wadsworth et al. 2017) that were capable of forming MSPs similar to those found at the SJ site. In addition, this airburst event may have directly produced MSPs from target material and altered atmospheric chemistry, creating an acidic atmosphere (Nenes et al. 2011) that may be linked to the enrichment in phosphorus. Productivity of aquatic ecosystems is controlled by the availability of phosphorus, and the processing of mineral aerosols by acids is a major source of water-soluble phosphorus. Phosphorus increases biotic productivity, especially in algae and other simple organisms (Mahowald et al. 2008).

Changes in Lake Environment in Response to Climate Oscillations at the Allerød-YD Transition

According to our age-depth model, the deposition of the BV, whose thickness is a little more than 1 cm (depth of 451.0–452.4 cm), represents a significant short-term cooling event, the Gerzensee climate oscillation (Ammann et al. 2013; van Raden et al. 2013), that resulted in a significant perturbation of the lake's ecosystem. The weathering index Th/K dropped to its minimum (figs. 3, 4), indicating a cold and/or dry climate, coinciding with a sudden increase in sediment transport from the lake's catchment to the lake basin. Low numbers of chironomid fossils (~2 head capsules per gram of dry sediment) were found in the BV sediment material (fig. 5*D*, 5*F*).

The LST layer is associated with nonlocal phosphorus-rich aerosol particles (figs. 3*A*, 4*F*) that adhered to the airborne tephra (fig. A11*B*). These aerosols were readily digestible by aquatic organisms (Nenes et al. 2011), thus supporting a sudden algal bloom and a sharp rise in cladoceran and chironomid abundances (Bunting et al. 2007). This scenario is also supported by an increase in LOI values (>12%).

The YDB is possibly associated with production of hydrogen sulfide, a by-product of microbial reduction of sulfate, as indicated by the formation of the pyritic framboids. This change in lake water chemistry could have resulted in sudden anoxia, a shift in redox conditions, and water saturation by sulfur (Ding et al. 2014). After that, pyritic framboids grew from biofilms on the lake floor or from the development of microenvironments around organic material, which preserved highly reactive organic compounds under euxinic conditions (Hethke et al. 2013). Anoxic conditions in bottom waters during mass-extinction events (Permian-Triassic boundary and Late Devonian) showed a major increase in the formation of framboids (De Vleeschouwer et al. 2013; Dustira et al. 2013). We interpret the abundance of framboids in the YDB layer at SJ as resulting indirectly from the deposition of glassy MSPs. After the decline in phosphorus levels (fig. 5*A*), chironomids (fig. 5*F*) reached a second peak in abundance during the deposition of the MSPs (~446 cm). A similar pattern with a short delay is shown in abundances of zooplankton (cladocerans in fig. 5*D*), chironomids associated with water macrophytes (*Corynoneura arctica*–type, *Psectrocladius sordidellus*–type), and quillwort (*Isoëtes*; fig. 5*E*). We also documented a distinct change in the composition of lake faunal species when chironomids typical for cold and oligotrophic water bodies (including *Tanytarsus lugens*–type and *T. pallidicornis*–type) were suppressed in favor of taxa preferring very cold and ultraoligotrophic conditions (increase in *Heterotrissocladius grimshawi*–type and *Micropsectra insignilobus*/*contracta*; first occurrence of *Micropsectra radialis* and *Paracladius*) and a decrease in relative abundance of pelagic cladocerans (especially *Daphnia* spp.). All this shows that climate deterioration at the YDB was manifested as a drop in the water/air temperature and a decrease in lake water level. On the other hand, no signal of drastic anoxia or eutrophication was found in cladoceran and chironomid assemblages. Such evidence, but on a significantly smaller scale, could be sup-

This content downloaded from 037.188.230.251 on September 25, 2018 23:51:12 PM
All use subject to University of Chicago Press Terms and Conditions (http://www.journals.uchicago.edu/t-and-c).

ported only by increased abundance of *Chironomus anthracinus*–type larvae at a depth of ~445.5 cm. These chironomids are tolerant of low oxygen concentrations and even anoxia for a few weeks.

The uppermost part of the depth interval analyzed for animal remains (444–442 cm; fig. 5) displays a record of oligotrophication after the YD onset, with decreasing species diversity in both cladocerans and chironomids. We suppose a continued decrease in the lake water level, which is supported by a dominance of littoral cladocerans and the presence of filamentous algae (*Zygnema* sp. and *Spirogyra* sp.) that covered the lake bottom (fig. 5*E*).

Changes in Catchment Vegetation and Biomass Burning

The YDB impact hypothesis posits that the cosmic impact/airburst triggered abrupt cooling at the onset of the YD episode (Firestone et al. 2007; Steffensen et al. 2008). Here we investigate whether our pollen data are consistent with this hypothesis. Pollen assemblages, extracted from the lake deposits, indicate that tundra vegetation, mixed with pines, dominated the SJ area during the Allerød interstadial that preceded deposition of the LST (fig. A5*A*). Before the GO, when the BV layer was deposited, the climate was warmer and provided abundant biomass that served as fuel during occasional wildfires, based on the observed charcoal density in the sediment (fig. A5*C*; Kletetschka and Banerjee 1995). An increase of *Artemisia* pollen in the GO indicates that sudden cooling occurred. After deposition of the GO material and the onset of cooler temperatures, low charcoal counts indicate low levels of biomass burning. After that, as local temperatures warmed, a denser vegetation cover in the SJ catchment at the YD onset (~12,757 ± 82 cal BP) provided sufficient biomass to produce a peak in charcoal concentrations (>125 μm; fig. A5*C*). However, the amplitude of the charcoal peak in the YDB layer falls within the overall variability of the entire lake record, meaning that wildfire activity was not significantly larger than earlier or later biomass-burning events. Even though charcoal concentrations are not significantly higher across the YDB in the SJ area, it is possible that local burning may have affected only grasses and leaves, which would not have produced large concentrations of charcoal.

The pollen record reflects significant changes in vegetation in the GO and YDB layers. Remnants of tree tissue, including *Pinus* stomata and carbonized pinewood (fig. A5*C*), indicate the presence of trees in the lake catchment. A significant pollen peak in *Artemisia*, an aggressive colonizer, indicates a major disturbance of the local biota near the GO, associated with a cooling event, while in the LST layer, a similar biotic disturbance is indicated by a sharp increase in birch tree pollen combined with a sharp decrease in pine pollen production (fig. A5*C*; de Klerk et al. 2008). During the YDB deposition, pine pollen decreases and birch pollen continues to increase. Thus, the most pronounced changes in terrestrial vegetation are synchronous with deposition of the YDB airburst-related spherules and the changes in the lake biota, representing the YD onset.

Conclusions

In this work, we developed a chronology with an easily identifiable stratigraphic marker (the BV layer in the midst of the GO) and LST. In combination with the radiocarbon dating, pollen, algae, and water invertebrate fauna record and high-resolution XRF elemental analyses, this allows a detailed chronostratigraphic investigation of climate, geochemistry, and biotic development across the Allerød-YD transition in the study lake and its catchment. We identified three disturbances of climate near the onset of the YD. The older climate change resulted from the GO (high sedimentation rate in the BV; fig. 2). Subsequently, the LST was found at a younger sedimentary level, followed by another layer of MSPs that correlates with the YDB layer at other sites across several continents, some of which also contain both meltglass and MSPs (Bunch et al. 2012). The composition of the tephra matches the middle sequence of LST eruption. Supporting evidence for a cosmic impact is the presence of Ni-containing MSPs (fig. 4*A*) and the presence of phosphorus-enriched MSPs. The proposed airburst (Firestone et al. 2007) would have provided enough energy to transport airborne dust to the SJ study site. The age of the YDB layer (12,727 ± 92 cal BP) falls within the previously published range for the YD onset (Bunch et al. 2012; Wittke et al. 2013). Furthermore, biotic changes recorded in the paleolake indicate significant cooling consistent with variations of the weathering index Th/K (fig. 3) immediately after deposition of the MSPs.

The LST layer co-occurs with an anomalously high accumulation of phosphorus, niobium, cerium, and lanthanum, along with evidence of major changes in the lake community, indicating possible eutrophication. The large influx of tephra-related phosphorus resulted in shifts in sensitive biocommunities of central European mountain lakes, substantially influencing the survivability of organisms/species, as shown at the SJ site. Changes in vegetation documented across Europe are reported to have been partly dia-

This content downloaded from 037.188.230.251 on September 25, 2018 23:51:12 PM
All use subject to University of Chicago Press Terms and Conditions (http://www.journals.uchicago.edu/t-and-c).

chronous in response to the onset of YD cooling (Steffensen et al. 2008). At the SJ site, pine and birch pollen records indicate a major vegetation shift in response to the YD cooling episode proposed to have been initiated by the YDB airburst event (appendix).

Cosmic airbursts are not well known, but large, locally destructive ones are predicted to recur with a frequency greater than one every few thousands of years (Collins et al. 2005; Boslough and Crawford 2008; Osinski et al. 2008; Napier 2010). One recent example was the airburst at Tunguska, Siberia, in 1908 that produced MSPs, nanodiamonds, and possibly meltglass while triggering extensive biomass burning and significant local devastation (Bunch et al. 2012; Kvasnytsya et al. 2013). In an apparent absence of impact craters, airbursts are indicated by the presence of these abundant markers, usually in discrete layers. Nearly all of these impact-related proxies are present in a discrete layer at SJ, consistent with an impact origin. In this work, our analyses of remanent magnetism in MSPs allow us to link the origin of at least some of the MSPs to lightning discharges within the impact-produced cloud of airborne dust. Other MSPs with no enhanced remanent magnetism are consistent with their direct production by the YDB impact event.

ACKNOWLEDGMENTS

This work was supported by the Czech Science Foundation within project 17-05935S, Ministry of Education, Youth and Sport grant LK21303, GA UK 687012, and grants RVO 67985831 and RVO 67985939. We thank H. Jilkova and L. Strnad for their help with Nb, P, S, and C concentration measurements. We thank T. Hrstka and N. Mészárosová for their help with SEM analyses. We thank J. Kennett and three anonymous reviewers for significantly improving the manuscript. G. Kletetschka designed the research and wrote the article; D. Vondrák performed depth correlation of the independent cores and LOI and chironomid remains analyses and interpreted the data; J. Hruba measured geochemical compositions; V. Prochazka identified the LST within the YDB section; L. Nabelek identified and separated MSPs from the magnetic fraction; H. Svitavská-Svobodová collected and interpreted the pollen data; P. Bobek collected and interpreted the charcoal data; Z. Horicka collected and interpreted the cladoceran data; J. Kadlec collected samples and provided advice; M. Takac designed the geochemical data collection system; and E. Stuchlik interpreted all bio- and geochemical proxies together.

REFERENCES CITED

Ammann, B. van Leeuwen, J. F. N.; van der Knaap, W. O.; Lischke, H.; Heiri, O.; and Tinner, W. 2013. Vegetation responses to rapid warming and to minor climatic fluctuations during the Late-Glacial Interstadial (GI-1) at Gerzensee (Switzerland). Palaeogeogr. Palaeoclimatol. Palaeoecol. 391B:40–59.

Baales, M.; Joris, O.; Street, M.; Bittmann, F.; Weninger, B.; and Wiethold, J. 2002. Impact of the late glacial eruption of the Laacher See volcano, central Rhineland, Germany. Quat. Res. 58(3):273–288.

Badyukov, D. D.; Ivanov, A. V.; Raitala, J.; and Khisina, N. R. 2011. Spherules from the Tunguska event site: could they originate from the Tunguska cosmic body? Geochem. Int. 49(7):641–653.

Bogaard, P., and Schmincke, H. U. 1985. Laacher See tephra: a widespread isochronous late Quaternary tephra layer in central and northern Europe. Geol. Soc. Am. Bull. 96(12):1554–1571.

Boslough, M. B. E., and Crawford, D. A. 2008. Low-altitude airbursts and the impact threat. Int. J. Impact Eng. 35(12): 1441–1448.

Brauer, A.; Endres, C.; and Negendank, J. F. W. 1999. Lateglacial calendar year chronology based on annually laminated sediments from Lake Meerfelder Maar, Germany. Quat. Int. 61:17–25.

Bronk Ramsey, C. 2009. Bayesian analysis of radiocarbon dates. Radiocarbon 51(1):337–360.

Bunch, T. E.; Hermes, R. E.; Moore, A. M. T.; Kennett, D. J.; Weaver, J. C.; Wittke, J. H.; DeCarli, P. S.; et al. 2012. Very high-temperature impact melt products as evidence for cosmic airbursts and impacts 12,900 years ago. Proc. Natl. Acad. Sci. USA 109(28):E1903–E1912.

Bunting, L.; Leavitt, P. R.; Gibson, C. E.; McGee, E. J.; and Hall, V. A. 2007. Degradation of water quality in Lough Neagh, Northern Ireland, by diffuse nitrogen flux from a phosphorus rich catchment. Limnol. Oceanogr. 52:354–369.

Collins, G. S.; Melosh, H. J.; and Marcus, R. A. 2005. Earth Impact Effects Program: a Web-based computer program for calculating the regional environmental consequences of a meteoroid impact on Earth. Meteorit. Planet. Sci. 40(6):817–840.

de Klerk, P.; Janke, W.; Kuehn, P.; and Theuerkauf, M. 2008. Environmental impact of the Laacher See eruption at a large distance from the volcano: integrated palaeoecological studies from Vorpommern (NE Germany). Palaeogeogr. Palaeoclimatol. Palaeoecol. 270(1–2):196–214.

De Vleeschouwer, D.; Rakociński, M.; Racki, G.; Bond, D. P. G.; Sobień, K.; and Claeys, P. 2013. The astronomical rhythm of Late-Devonian climate change (Kowala section, Holy Cross Mountains, Poland). Earth Planet. Sci. Lett. 365:25–37.

Ding, H.; Yao, S. P.; and Chen, J. 2014. Authigenic pyrite formation and re-oxidation as an indicator of an unsteady-

This content downloaded from 037.188.230.251 on September 25, 2018 23:51:12 PM
All use subject to University of Chicago Press Terms and Conditions (http://www.journals.uchicago.edu/t-and-c).

state redox sedimentary environment: evidence from the intertidal mangrove sediments of Hainan Island, China. Cont. Shelf Res. 78:85–99.

Dustira, A. M.; Wignall, P. B.; Joachimski, M.; Blomeier, D.; Hartkopf-Froder, C.; and Bond, D. P. G. 2013. Gradual onset of anoxia across the Permian-Triassic Boundary in Svalbard, Norway. Palaeogeogr. Palaeoclimatol. Palaeoecol. 374:303–313.

Fayek, M.; Anovitz, L. M.; Allard, L. F.; and Hull, S. 2012. Framboidal iron oxide: chondrite-like material from the black mat, Murray Springs, Arizona. Earth Planet. Sci. Lett. 319:251–258.

Firestone, R. B.; West, A.; Kennett, J. P.; Becker, L.; Bunch, T. E.; Revay, Z. S.; Schultz, P. H.; et al. 2007. Evidence for an extraterrestrial impact 12,900 years ago that contributed to the megafaunal extinctions and the Younger Dryas cooling. Proc. Natl. Acad. Sci. USA 104(41):16,016–16,021.

French, B. M. 1998. Traces of catastrophe: a handbook of shock-metamorphic effects in terrestrial meteorite impact structures. LPI Contribution no. 954. Houston, Lunar and Planetary Institute.

Hethke, M.; Fürsich, F. T.; Jiang, B. Y.; and Klaus, R. 2013. Oxygen deficiency in Lake Sihetun; formation of the Lower Cretaceous Liaoning Fossillagerstätte (China). J. Geol. Soc. Lond. 170(5):817–831.

Hošek, J.; Pokorný, P.; Kubovčík, V.; Horáček, I.; Žáčková, P.; Kadlec, J.; Rojik, F.; Lisá, L.; and Bučkuliaková, S. 2014. Late glacial climatic and environmental changes in eastern-central Europe: correlation of multiple biotic and abiotic proxies from the Lake Švarcenberk, Czech Republic. Palaeogeogr. Palaeoclimatol. Palaeoecol. 396: 155–172.

Israde-Alcántara, I.; Bischoff, J. L.; Dominguez-Vázquez, G.; Li, H. C.; DeCarli, P. S.; Bunch, T. E.; Wittke, J. H.; et al. 2012. Evidence from central Mexico supporting the Younger Dryas extraterrestrial impact hypothesis. Proc. Natl. Acad. Sci. USA 109(13):E738–E747.

Juvigné, E.; Kozarski, S.; and Nowaczyk, S. 1995. The occurrence of Laacher See tephra in Pomerania, NW Poland. Boreas 24:225–231.

Kennett, D. J.; Kennett, J. P.; West, A.; Mercer, C.; Que Hee, S. S.; Bement, L.; Bunch, T. E.; Sellers, M.; and Wolbach, W. S. 2009. Nanodiamonds in the Younger Dryas boundary sediment layer. Science 323(5910):94–94.

Kennett, J. P.; Kennett, D. J.; Culleton, B. J.; Tortosa, J. E. A.; Bischoff, J. L.; Bunch, T. E.; Daniel, I. R., Jr.; et al. 2015. Bayesian chronological analyses consistent with synchronous age of 12,835–12,735 Cal BP for Younger Dryas boundary on four continents. Proc. Natl. Acad. Sci. USA 112(32):E4344–E4353.

Kletetschka, G., and Banerjee, S. K. 1995. Magnetic stratigraphy of Chinese loess as a record of natural fires. Geophys. Res. Lett. 22(11):1341–1343.

Kletetschka, G.; Procházka, V.; Fantucci, R.; and Trojek, T. 2017. Survival response of *Larix sibirica* to the Tunguska explosion. Tree-Ring Res. 73(2):75–90.

Kurbatov, A. V.; Mayewski, P. A.; Steffensen, J. P.; West, A.; Kennett, D. J.; Kennett J. P.; Bunch, T. E.; et. al. 2010. Discovery of a nanodiamond-rich layer in the Greenland ice sheet. J. Glaciol. 56(199):747–757.

Kvasnytsya, V.; Wirth, R.; Dobrzhinetskaya, L.; Matzel, J.; Jacobsen, B.; Hutcheon, I.; Tappero, R.; and Kovalyukh, M. 2013. New evidence of meteoritic origin of the Tunguska cosmic body. Planet. Space Sci. 84:131–140.

LeCompte, M. A.; Goodyear, A. C.; Demitroff, M. N.; Batchelor, D.; Vogel, E. K.; Mooney, C.; Rock, B. N.; and Seidel, A. W. 2012. Independent evaluation of conflicting microspherule results from different investigations of the Younger Dryas impact hypothesis. Proc. Natl. Acad. Sci. USA 109(44):E2960–E2969.

Mahaney, W. C.; Keiser, L.; Krinsley, D.; Kalm, V.; Beukens, R.; and West, A. 2013. New evidence from a black mat site in the northern Andes supporting a cosmic impact 12,800 years ago. J. Geol. 121(4):309–325.

Mahowald, N.; Jickells, T. D.; Baker, A. R.; Artaxo, P.; Benitez-Nelson, C. R.; Bergametti, G.; Bond, T. C.; et al. 2008. Global distribution of atmospheric phosphorus sources, concentrations and deposition rates, and anthropogenic impacts. Glob. Biogeochem. Cycles 22(4): GB4026. doi:10.1029/2008GB003240.

Mentlík, P.; J. Minár, J.; Břízová, E.; Lisá, L.; Tábořík, P.; and Stacke, V. 2010. Glaciation in the surroundings of Prášilské Lake (Bohemian Forest, Czech Republic). Geomorphology 117(1–2):181–194.

Moore, C. R.; West, A.; LeCompte, M. A.; Brooks, M. J.; Daniel, I. R., Jr.; Goodyear, A. C.; Ferguson, T. A.; et al. 2017. Widespread platinum anomaly documented at the Younger Dryas onset in North American sedimentary sequences. Sci. Rep. 7:44031. doi:10.1038/srep44031.

Napier, W. M. 2010. Palaeolithic extinctions and the Taurid Complex. Mon. Notes R. Astron. Soc. 405(3):1901–1906.

Nenes, A.; Krom, M. D.; Mihalopoulos, N.; Van Cappellen, P.; Shi, Z.; Bougiatioti, A.; Zarmpas, P.; and Herut, B. 2011. Atmospheric acidification of mineral aerosols: a source of bioavailable phosphorus for the oceans. Atmos. Chem. Phys. 11(13):6265–6272.

Neugebauer, I.; Brauer, A.; Dräger, N.; Dulski, P.; Wulf, S.; Plessen, B.; Mingram, J.; Herzschuh, U.; and Brande, A. 2012. A Younger Dryas varve chronology from the Rehwiese palaeolake record in NE-Germany. Quat. Sci. Rev. 36:91–102.

Osinski, G. R.; Kieniewicz, J.; Smith, J. R.; Boslough, M. B. E.; Eccleston, M.; Schwarcz, H. P.; Kleindienst, M. R.; Haldemann, A. F. C.; and Churcher, C. S. 2008. The Dakhleh Glass: product of an impact airburst or cratering event in the Western Desert of Egypt? Meteorit. Planet. Sci. 43(12):2089–2106.

Parnell, A. C.; Phillips, D. L.; Bearhop, S.; Semmens, B. X.; Ward, E. J.; Moore, J. W.; Jackson, A. L.; Grey, J.; Kelly, D. J.; and Inger, R. 2013. Bayesian stable isotope mixing models. Environmetrics 24(6):387–399.

Petaev, M. I.; Huang, S. C.; Jacobsen, S. B.; and Zindler, A. 2013. Large Pt anomaly in the Greenland ice core points to a cataclysm at the onset of Younger Dryas. Proc. Natl. Acad. Sci. USA 110(32):12,917–12,920.

This content downloaded from 037.188.230.251 on September 25, 2018 23:51:12 PM
All use subject to University of Chicago Press Terms and Conditions (http://www.journals.uchicago.edu/t-and-c).

Pinter, N.; Scott, A. C.; Daulton, T. L.; Podoll, A.; Koeberl, C.; Anderson, R. S.; and Ishman, S. E. 2011. The Younger Dryas impact hypothesis: a requiem. Earth-Sci. Rev. 106(3–4):247–264.

Pliler, R., and Adams, J. A. S. 1962. The distribution of thorium and uranium in a Pennsylvanian weathering profile. Geochim. Cosmochim. Acta 26:1137–1146.

Rach, O.; Brauer, A.; Wilkes, H.; and Sachse, D. 2014. Delayed hydrological response to Greenland cooling at the onset of the Younger Dryas in western Europe. Nat. Geosci. 7(2):109–112.

Rasmussen, S. O.; Bigler, M.; Blockley, S. P.; Blunier, T.; Buchardt, S. L.; Clausen, H. B.; Cvijanovic, I.; et al. 2014. A stratigraphic framework for abrupt climatic changes during the Last Glacial period based on three synchronized Greenland ice-core records: refining and extending the INTIMATE event stratigraphy. Quat. Sci. Rev. 106:14–28.

Rausch, J.; Grobety, B.; and Vonlanthen, P. 2015. Eifel maars: quantitative shape characterization of juvenile ash particles (Eifel Volcanic Field, Germany). J. Volcanol. Geotherm. Res. 291:86–100.

Reimer, P. J.; Bard, E.; Bayliss, A.; Beck, J. W.; Blackwell, P. G.; Bronk Ramsey, C.; Brown, D. M.; et al. 2013. Selection and treatment of data for radiocarbon calibration: an update to the international calibration (INTCAL) criteria. Radiocarbon 55(4):1923–1945.

Riede, F.; Bazely, O.; Newton, A. J.; and Lane, C. S. 2011. A Laacher See–eruption supplement to Tephrabase: investigating distal tephra fallout dynamics. Quat. Int. 246:134–144.

Robock, A. 2000. Volcanic eruptions and climate. Rev. Geophys. 38(2):191–219.

Schmincke, H.-U.; Park, C.; and Harms, E. 1999. Evolution and environmental impacts of the eruption of Laacher See volcano (Germany) 12,900 a BP. Quat. Int. 61:61–72.

Shevtsov, B. M.; Firstov, P. P.; Cherneva, N. V.; Holzworth, R. H.; and Akbashev, R. R. 2016. Lightning and electrical activity during the Shiveluch volcano eruption on 16 November 2014. Nat. Hazards Earth Syst. Sci. 16(3):871–874.

Steffensen, J. P.; Andersen, K. K.; Bigler, M.; Clausen, H. B.; Dahl-Jensen, D.; Fischer, H.; Goto-Azuma, K.; et al. 2008. High-resolution Greenland ice core data show abrupt climate change happens in few years. Science 321(5889):680–684.

Taylor, G. J.; Stopar, J. D.; Boynton, W. V.; Karunatillake, S.; Keller, J. M.; Brückner, J.; Wänke, H.; et al. 2006. Variations in K/Th on Mars. J. Geophys. Res. Planets 111:E03S06. doi:10.1029/2006JE002676.

Turney, C. S. M.; Van Den Burg, K.; Wastegård, S.; Davies, S. M.; Whitehouse, N. J.; Pilcher, J. R.; and Callaghan, C. 2006. North European last glacial-interglacial transition (LGIT; 15–9 ka) tephrochronology: extended limits and new events. J. Quat. Sci. 21:335–345.

van Hoesel, A.; Hoek, W. Z.; Braadbaart, F.; van der Plicht, J.; Pennock, G. M.; and Drury, M. R. 2012. Nanodiamonds and wildfire evidence in the Usselo horizon postdate the Allerød-Younger Dryas boundary. Proc. Natl. Acad. Sci. USA 109(20):7648–7653.

van Hoesel, A.; Hoek, W. Z.; Pennock, G. M.; and Drury, M. R. 2014. The Younger Dryas impact hypothesis: a critical review. Quat Sci. Rev. 83:95–114.

van Raden, U. J.; Colombaroli, D.; Gilli, A.; Schwander, J.; Bernasconi, S. M.; van Leeuwen, J.; Leuenberger, M.; and Eicher, U. 2013. High-resolution late-glacial chronology for the Gerzensee lake record (Switzerland): $\delta^{18}O$ correlation between a Gerzensee-stack and NGRIP. Palaeogeogr. Palaeoclimatol. Palaeoecol. 391B:13–24.

Wadsworth, F. B.; Vasseur, J.; Llewellin, E. W.; Genareau, K.; Cimarelli, C.; and Dingwell, D. B. 2017. Size limits for rounding of volcanic ash particles heated by lightning. J. Geophys. Res. Solid Earth 122(3):1977–1989.

Wasilewski, P. 1981. Magnetization of small iron-nickel spheres. Phys. Earth Planet. Inter. 26(1–2):149–161.

Wasilewski, P., and Kletetschka, G. 1999. Lodestone: natures only permanent magnet—what it is and how it gets charged. Geophys. Res. Lett. 26(15):2275–2278.

Wittke, J. H.; Weaver, J. C.; Bunch, T. E.; Kennett, J. P.; Kennett, D. J.; Moore, A. M. T.; Hillman, G. C.; et al. 2013. Evidence for deposition of 10 million tonnes of impact spherules across four continents 12,800 y ago. Proc. Natl. Acad. Sci. USA 110:E2088–E2097. doi:10.1073/pnas.1301760110.

Wolbach, W. S.; Ballard, J. P.; Mayewski, P. A.; Adedeji, V.; Bunch, T. E.; Firestone, R. B.; French, T. A.; et al. 2018*a*. Extraordinary biomass-burning episode and impact winter triggered by the Younger Dryas cosmic impact ~12,800 years ago. 1. Ice cores and glaciers. J. Geol. 126(2):165–184.

Wolbach, W. S.; Ballard, J. P.; Mayewski, P. A.; Parnell, A. C.; Cahill, N.; Adedeji, V.; Bunch, T. E.; et al. 2018*b*. Extraordinary biomass-burning episode and impact winter triggered by the Younger Dryas cosmic impact ~12,800 years ago. 2. Lake, marine, and terrestrial sediments. J. Geol. 126(2):185–205.

Wu, Y. Z.; Sharma, M.; LeCompte, M. A.; Demitroff, M. N.; and Landis, J. D. 2013. Origin and provenance of spherules and magnetic grains at the Younger Dryas boundary. Proc. Natl. Acad. Sci. USA 110(38):E3557–E3566.

Wulf, S.; Ott, F.; Słowiński, M.; Noryśkiewicz, A. M.; Dräger, N.; Martin-Puertas, C.; Czymzik, M.; et al. 2013. Tracing the Laacher See tephra in the varved sediment record of the Trzechowskie palaeolake in central northern Poland. Quat. Sci. Rev. 76:129–139.

This content downloaded from 037.188.230.251 on September 25, 2018 23:51:12 PM
All use subject to University of Chicago Press Terms and Conditions (http://www.journals.uchicago.edu/t-and-c).